

Quantum Monte Carlo simulation of thermodynamic properties of $SU(2N)$ ultracold fermions in optical lattices

Zhichao Zhou,¹ Zi Cai,² Congjun Wu,³ and Yu Wang^{1,*}

¹*School of Physics and Technology, Wuhan University, Wuhan 430072, China*

²*Institute for Quantum Optics and Quantum Information,
Austrian Academy of Sciences, 6020 Innsbruck, Austria*

³*Department of Physics, University of California, San Diego, CA 92093, USA*

We have systematically studied the thermodynamic properties of a two-dimensional half-filled $SU(2N)$ Hubbard model on a square lattice by using the determinant quantum Monte Carlo method. The entropy-temperature relation, the isoentropy curve, and the probability distribution of the onsite occupation number are calculated in both $SU(4)$ and $SU(6)$ cases, which exhibit prominent features of the Pomeranchuk effect. We analyze these thermodynamic behaviors based on charge and spin energy scales. In the charge channel, the interaction strength that marks the crossover from the weak to strong interaction regimes increases with the number of fermion components. In the spin channel, increasing the number of fermion components enhances quantum spin fluctuations, which is shown in the simulations of uniform spin susceptibilities and antiferromagnetic structure factors.

PACS numbers: 71.10.Fd, 03.75.Ss, 37.10.Jk, 71.27.+a

I. INTRODUCTION

In condensed matter physics, the goal of generalizing $SU(2)$ lattice fermion or spin models to those with high symmetries of $SU(N)^{1-3}$ or $Sp(N)^{4,5}$, was originally to employ the systematic $1/N$ -expansion to handle strong correlation physics, especially in the cases with doping or frustrations. Generally speaking, the large symmetries of $SU(N)$ and $Sp(N)$ enhance quantum spin fluctuations and suppress the antiferromagnetic (AF) order^{1,2,5}. Various exotic quantum paramagnetic phases have been proposed based on the large- N method, including various valence bond solid states and quantum spin liquid states⁶⁻¹⁰. However, in conventional solid states, the $SU(N)$ symmetry is rare and thus the $SU(N)$ Hubbard or Heisenberg models are purely of academic interest.

With the rapid development of the ultracold atom experiments, the realization of multi-component fermionic Hubbard models with the $SU(2N)$ or $Sp(2N)$ symmetry has become a realistic goal (the number of fermion components due to the hyperfine spin degree of freedom is naturally an even number). It was proposed that the simplest $Sp(2N)$ and $SU(2N)$ Hubbard models with $2N = 4$ can be realized in the hyperfine spin- $\frac{3}{2}$ alkali and alkaline-earth atoms^{11,12}. In these spin- $\frac{3}{2}$ Hubbard models, an exact $Sp(4)$ spin symmetry exists without any fine-tuning of parameters, which is further enlarged to $SU(4)$ when the interactions do not rely on hyperfine spin. The alkaline-earth atoms, *e.g.*, ^{173}Yb and ^{87}Sr , have a closed shell of valence electrons and thus their hyperfine spins are simply nuclear spins. The interactions between the atoms with different hyperfine spins are insensitive to the nuclear spins, leading to the $SU(2N)$ symmetry with $2N$ being the number of fermion components^{13,14}.

Recently, significant progress has been made in the experiment of ultracold alkaline-earth fermions with large hyperfine spins. The ^{173}Yb and ^{87}Sr atoms have been

cooled down to quantum degenerate temperatures¹⁵⁻¹⁷, revealing the $SU(6)$ and $SU(10)$ symmetries respectively. Furthermore, an $SU(6)$ single-band fermionic Hubbard model has also been realized with ^{173}Yb atoms in a three-dimensional optical lattice¹⁸. Beyond single-band case, the spin-exchange interactions have recently been observed in the two-orbital $SU(6)$ and $SU(10)$ fermion system respectively^{19,20}. Also the number of spin components can be tuned experimentally²¹. Theoretically, the novel symmetries of the multi-component Hubbard model can give rise to the novel superfluidity²²⁻²⁸ and exotic quantum magnetism²⁹⁻³⁸.

In ultracold atom experiments, achieving low enough temperature regime below the spin superexchange scale has been considered a benchmark for simulating strongly correlated quantum systems. Despite numerous efforts by experimentalists, achieving this temperature regime is still out of reach and remains one of the most challenging problems in this field. So far, ultracold fermions in optical lattices have been cooled down to temperature regime below the hopping energy scale, $T \sim t$. One of the promising schemes for further cooling the system into spin superexchange scale $T \sim J$ is known as interaction-induced adiabatic cooling³⁹, a cooling scheme by adiabatically increasing interactions. This cooling scheme utilizes the Pomeranchuk effect which was originally proposed in ^3He systems. However, for a two-component Hubbard model in conventional lattices, the Pomeranchuk effect is weak due to the antiferromagnetic correlations in the $SU(2)$ Mott insulator. It is still controversial whether the system can be cooled down to spin superexchange temperature by Pomeranchuk cooling³⁹⁻⁴². As we show below, the multi-component $SU(2N)$ Hubbard model significantly facilitates the Pomeranchuk cooling, cooling the system down to the temperature scale of J from an initial temperature that is currently accessible in experiments.

This paper extends the previous work reported in Ref.

[43]. We have performed detailed determinant quantum Monte Carlo (DQMC) simulations of thermodynamic properties of the half-filled SU(2N) Hubbard model with $2N = 4$ and 6 in the temperature regime $J < T < t$. We calculated the entropy-temperature relation and isoentropy curves, which show the enhancement of entropy with increasing interaction strength in the intermediate temperature regime, *i.e.*, the Pomeranchuk effect. The probability distributions of the onsite occupation number show the enhancement of particle localization as temperature increases in the low and intermediate temperature regimes. The uniform spin susceptibilities and AF structure factors are also calculated.

The rest part of this paper is organized as follows. In Section II, we introduce the definition of the SU(2N) Hubbard model. A discussion of the charge and spin energy scales of the half-filled SU(2N) Hubbard model is followed in Section III. The parameters of the DQMC simulations are given in Section IV. In Section V, we present the results of DQMC study on the thermodynamic properties of the half-filled SU(4) and SU(6) Hubbard models. In Section VII, the magnetic properties at finite temperatures are investigated. Conclusions are drawn in Section VIII.

II. THE SU(2N) HUBBARD MODEL

Since naturally the number of fermion components due to the hyperfine spin degree of freedom is an even number, we only consider Hubbard model with SU(2N) symmetry. At half-filling, an SU(2N) Hubbard model is defined by the lattice Hamiltonian:

$$H = -t \sum_{\langle i,j \rangle, \alpha} \{c_{i\alpha}^\dagger c_{j\alpha} + h.c.\} + \frac{U}{2} \sum_i (n_i - N)^2, \quad (1)$$

where $\langle i, j \rangle$ denotes nearest neighbors and the sum runs over sites of a two-dimensional square lattice; α represents spin indices running from 1 to $2N$; n_i is the particle number operator on site i defined by $n_i = \sum_{\alpha=1}^{2N} c_{i\alpha}^\dagger c_{i\alpha}$; t and U are the nearest neighbor hopping integral and the onsite interaction, respectively.

This definition of Hubbard Hamiltonian Eq.(1) offers several advantages. In the atomic limit ($t = 0$), consider a half-filled lattice with N particles per site, the energy cost of moving a particle from one site to its neighboring site is U , which is independent of N . Due to half-filling, the chemical potential μ vanishes in this grand canonical Hamiltonian. Eq.(1) also has particle-hole symmetry in bipartite lattices, which removes the sign problem in DQMC simulations for an arbitrary value of $2N$.

In terms of the multiplets of SU(2N) fermions in the fundamental representation, the generators of the SU(2N) group can be written as

$$S_{\alpha\beta}(i) = c_{\alpha}^\dagger(i)c_{\beta}(i) - \frac{\delta_{\alpha\beta}}{2N} \sum_{\gamma=1}^{2N} c_{\gamma}^\dagger(i)c_{\gamma}(i), \quad (2)$$

where α and β run from 1 to $2N$. The generators defined above are not independent of each other, since the diagonal operators satisfy the relation, $\sum_{\alpha} S_{\alpha\alpha}(i) = 0$. Nevertheless, the definition of operators, Eq.(2), results in a simple commutation relation

$$[S^{\alpha\beta}, S^{\gamma\delta}] = \delta_{\beta\gamma} S^{\alpha\delta} - \delta_{\alpha\delta} S^{\gamma\beta}. \quad (3)$$

For convenience, we define the structure factor $S_{su(2N)}(\vec{q})$ as

$$S_{su(2N)}(\vec{q}) = \frac{1}{L^2} \sum_{i,j} e^{i\vec{q}\cdot\vec{r}} S_{spin}(i,j), \quad (4)$$

where \vec{r} is the relative vector between sites i and j . $S_{spin}(i,j)$ is the SU(2N) version of equal-time spin-spin correlation functions defined by

$$S_{spin}(i,j) = \frac{1}{(2N)^2 - 1} \sum_{\alpha,\beta} \langle S_{\alpha\beta,i} S_{\beta\alpha,j} \rangle. \quad (5)$$

III. THE CHARGE AND SPIN ENERGY SCALES

Before going to the results of DQMC simulation, let us present a qualitative understanding of the physics of the half-filled Hubbard model on a square lattice. The charge channel and spin channel are characterized by two energy scales Δ_c and Δ_s , respectively, which will be discussed in both the weak and strong interaction regimes below.

A. The weak interaction regime and the atomic limit

We first consider the weak interaction limit ($U \rightarrow 0$). In this regime, the underlying Fermi surface plays an important role, which possesses the diamond shape and thus exhibits perfect nesting. The key physics then arises from the Fermi surface nesting: the spin susceptibility in the non-interacting limit divergences logarithmically, and thus an infinitesimal repulsive interaction generates AF long-range-order. In this case, the gapped quasi-particle excitations carry both charge and spin quantum numbers. The charge and spin energy scales are identical in this regime as⁴⁴

$$\Delta_s/t = \Delta_c/t = 4\pi^2 e^{-\sqrt{2\pi t/U}}. \quad (6)$$

Certainly, in the weak interaction regime, the system is a weak insulator. Although it is gapped, charge fluctuations cannot be neglected. On the contrary, in the atomic limit ($t = 0$, or, $U \rightarrow +\infty$), the Fermi surface completely disappears, and we need to use the local moment picture. At zero temperature, charge fluctuations are completely frozen. In the Mott-insulating state, we use the single-particle gap to denote the charge fluctuations, *i.e.*, the

energy cost by adding or removing a particle from the Mott-insulating state. It is the energy difference between the two energy levels $\Delta_c = E_{n_i=N+1} - E_{n_i=N}$ which equals $\frac{U}{2}$ in the atomic limit. Since the hopping process is completely suppressed, the AF exchange energy $J = 0$, *i.e.*, the spin energy scale Δ_s is zero in the atomic limit.

B. The strong interaction regime

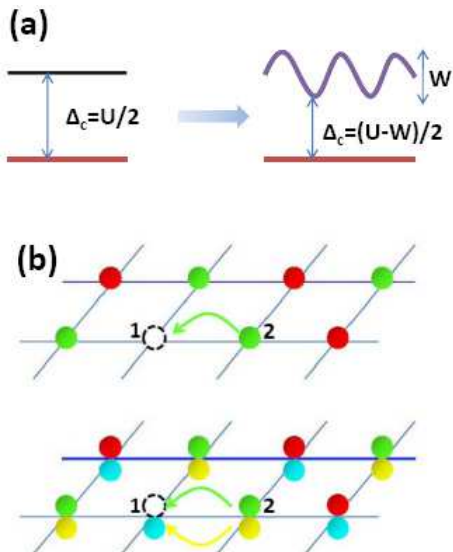


FIG. 1: (a) Energy dispersion of a charge excitation on the background of the half-filled Mott-insulating state: (left) the atomic limit with $t/U = 0$, (right) $t/U \ll 1$. (b) Sketches of a hole hopping in the SU(2) (up) and SU(4) (down) AF backgrounds, respectively. (Fig 1 (b) is from Ref. [43].)

Let us consider the strong interaction regime in which U is large but not strong enough to completely suppress charge fluctuations, *i.e.*, $t/U \ll 1$. Let us consider the charge energy scale Δ_c by adding an extra particle (hole) onto the background of the Mott-insulating state. As shown in Fig. 1 (a), the propagation of the particle (hole) expands the excitation energy level at $U/2$ in the atomic limit into an energy band. The charge gap corresponds to the band bottom and thus is lowered to

$$\Delta_c = \frac{U}{2} - \frac{W}{2}, \quad (7)$$

where W is the band width and is determined by the hopping process of the extra particle (hole).

In Fig. 1 (b), we compare the hopping process of an extra hole in the half-filled SU(2) and SU(4) Mott insulators. In the SU(4) case, there are much more routes for the hole to hop from one site to its neighboring site than it does in the SU(2) case. Typically speaking, the number of hopping process for an extra particle or hole under the half-filled Mott-insulating background scales as N , thus we estimate $W \propto Nt$. The mobility of the extra hole is

greatly enhanced in the SU(2N) Mott-insulating state. Consequently, the charge energy scale Δ_c is significantly lowered with increasing $2N$. Naively, we could estimate that Δ_c vanishes at

$$U_c \approx Nt. \quad (8)$$

Certainly, due to Fermi surface nesting, Δ_c does not vanish even in the weak interaction regime but becomes exponentially small. Nevertheless, U_c sets up a scale of interaction strength to separate the regimes of the Fermi surface nesting and the local moments.

The low energy physics in the strong interaction regime is described by the SU(2N) generalization of the Heisenberg model:

$$H = J \sum_{\alpha, \beta, [\vec{i}\vec{j}]} S_{\alpha\beta, \vec{i}} S_{\beta\alpha, \vec{j}}, \quad (9)$$

where the SU(2N) spin operators are defined in Eq.(2). J describes the strength of spin superexchange energy scale which can be viewed as the spin energy scale Δ_s . The second order perturbation theory yields $J = 4t^2/U$ which decreases as U increases. Noting that $\Delta_s \approx 4\pi^2 t e^{-2\pi\sqrt{t/U}}$ in the weak interaction regime, which increases with U , there should exist a peak in the intermediate interaction regime.

C. Effect of finite temperatures

When the fermion system is deep in the Mott-insulating state, in the low temperature regime $T \ll \Delta_s$, charge fluctuations are strongly suppressed, and the physics is dominated by spin superexchange process. Therefore quantum spin fluctuations play an important role in determining the magnetic properties of the Mott-insulating state at low temperatures. On the contrary, at high temperatures $T \gg \Delta_c$, quantum fluctuations give way to thermal fluctuations, which suppress quantum correlations, and thus interaction effects can be neglected. In the intermediate temperature regime $\Delta_s < T < \Delta_c$, T is high enough to suppress the AF correlations, but not sufficient to defreeze charge fluctuations. Both quantum and thermal fluctuations are important in the intermediate temperature regime, and the interplay between them gives rise to interesting phenomena and universal properties⁴⁵.

IV. THE DQMC METHOD

The DQMC method is a widely used non-perturbative method for studying strongly correlated fermion systems⁴⁶⁻⁵³. Provided that there is no sign problem, DQMC is known to be a well-controlled and unbiased method, which yields asymptotically exact results. One of the most remarkable DQMC results is the AF long-range order in the ground state of 2D SU(2) half-filled

Fermi-Hubbard model on a square lattice^{48,49,54}. In the subsequent sections, we will use the DQMC method to simulate thermodynamic properties of the half-filled $SU(2N)$ Hubbard model in different regimes of temperature T and interaction U . We will also show how those results are related to the two energy scales Δ_s and Δ_c analyzed in previous section.

Considering the error accumulation from matrix multiplications and simulation time, the lowest temperature in simulations is set as $T_L/t = 0.1$ (with $\beta = t/T_L = 10$). The Suzuki-Trotter decomposition is used in which the error is proportional to the cube of time discretization parameter $(\Delta\tau)^3$. $\Delta\tau$ is set from 0.02 to 0.05 in the temperature regime $T_L/t < T/t < 0.5$, and the convergence with respect to the scalings of $\Delta\tau$ has been checked.

A Hubbard-Stratonovich (HS) transformation that decomposes the onsite Hubbard interaction term in the density channel⁷ preserves the $SU(2)$ symmetry of the Hubbard model, which can also be generalized to the $SU(2N)$ Hubbard model. The discrete HS decomposition with an Ising field only applies to the spin- $\frac{1}{2}$ case^{47,48}. For the cases of $SU(4)$ and $SU(6)$, an exact discrete decomposition has been developed in Ref. [55], which is explained in Appendix and employed in our simulations. The simulated system is a $L \times L$ square lattice with $L = 10$. We focus on the parameter regimes of $0.1 < T/t < 10$ and $2 \leq U/t \leq 12$. For a typical data point, we use 10 QMC bins each of which includes 2000 warm-up steps and 8000 measurement steps. We collect data once in each time slice. In our simulations, t is set to unity and then the Hubbard U and temperature T are given in the unit of t .

V. THERMODYNAMIC PROPERTIES OF HALF-FILLED $SU(2N)$ HUBBARD MODEL

In this section, we present the simulations of thermodynamic properties of the half-filled $SU(2N)$ Hubbard model with $2N = 4$ and 6 on a square lattice, including the entropy-temperature relation, and the Pomeranchuk effect.

A. The entropy-temperature relation

In cold atom experiments, entropy is actually a more physical quantity than temperature to characterize the system. Below we present the simulated entropy in the half-filled $SU(4)$ and $SU(6)$ Hubbard models. The parameters of simulation are chosen in the regimes of $0.1 < T/t < 10$ and $2 \leq U/t \leq 12$, which are of interest in experiment. The simulated entropy per particle (not per site) is defined by $S_{SU(2N)} = S/(NL^2)$, where S is the total entropy in the lattice. The following formula is

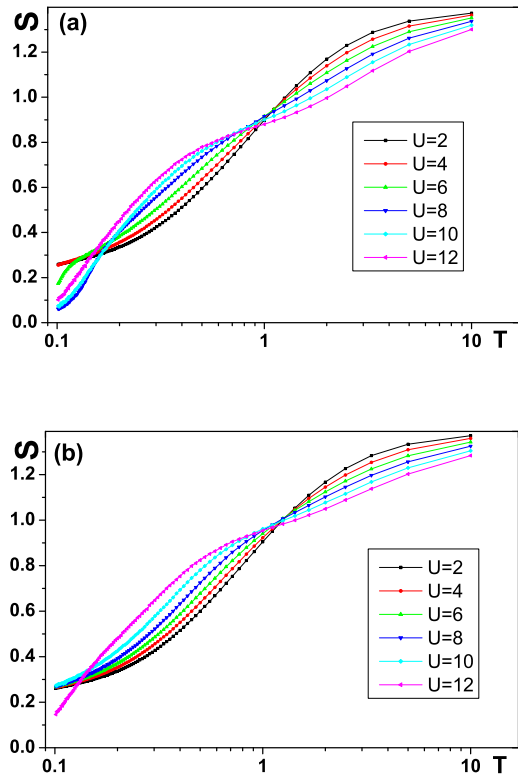


FIG. 2: The entropy per particle as a function of T for different values of U in (a) $SU(4)$ and (b) $SU(6)$ Hubbard models. The system size is $L \times L$ with $L = 10$.

employed to calculate $S_{SU(2N)}$:

$$\frac{S_{SU(2N)}(T)}{k_B} = \ln 4 + \frac{E(T)}{T} - \int_T^\infty dT' \frac{E(T')}{T'^2}, \quad (10)$$

where $\ln 4$ is the entropy at infinite temperature; $E(T)$ denotes the internal energy per particle at temperature T .

In Fig. 2, we show the entropy (per particle) of $SU(4)$ and $SU(6)$ fermions as a function of T for various values of U . In both cases, the curves cross at two *typical* temperatures T_l (low) and T_h (high) which divide the temperature into three different regimes. Let us first look at the $SU(4)$ case as follows.

The low temperature regime $T_L < T < T_l$ In this regime, the dependence of the entropy per particle $S_{SU(2N)}$ on U is non-monotonic, which can be understood by the competition between the spin energy scale Δ_s and the charge energy scale Δ_c as explained below.

For weak interactions $U/t < 4$, $S_{SU(4)}$ is insensitive to U . As explained in section III A, the physics in this regime is characterized by the Fermi surface nesting Δ_c and Δ_s which are equal and are smaller than $T_L/t \approx 0.1$ (the lowest temperature reached in our simulations), and thus interaction effects are unimportant. $S_{SU(4)}$ is then

approximately the same as that in the non-interacting limit. The non-zero residue entropy is due to the finite size effect which is caused by the degeneracy of single particle states right located on the Fermi surface. As U increases, Δ_c increases faster than Δ_s , while Δ_s quickly reaches its maximum. In this interaction regime, the relation $\Delta_c > \Delta_s > T$ holds, and thus increasing U freezes charge fluctuations but enhances AF correlations. Even though there cannot be true long-range AF ordering at finite temperatures in 2D, the AF correlation length scales as $e^{-\frac{\Delta_s}{T}}$. Consequently, $S_{SU(4)}$ drops with increasing U and the residue entropy, in principle, approaches zero. If U continues to increase and reaches the strong interaction regime, say, $U/t > 8$, $\Delta_c \simeq U/2$ increases while $\Delta_s \simeq J = 4t^2/U$ decreases. Thus the relation $\Delta_c \gg T \gg \Delta_s$ holds. T is low enough to freeze charge fluctuations but high enough to disorder AF correlations. Therefore, increasing U (or equivalently, decreasing Δ_s) enhances the entropy at a fixed T in the low temperature regime.

Intermediate temperature regime $T_l < T < T_h$ In this temperature regime, $S_{SU(4)}$ monotonically increases with U at a fixed T . At small U the system is in the weak Mott-insulating state with small values of Δ_s and Δ_c , which is very close to a Fermi liquid state. The system enters the solid-like strong Mott state at large U , where the physics is mostly local-moment-like. The increase of entropy with U means that the liquid-like state is more ordered than the solid-like state, known as the Pomeranchuk effect. In this temperature regime, T is high enough compared to Δ_s , and thus thermal fluctuations suppress magnetic correlations, while it remains smaller than Δ_c , such that charge fluctuations are still frozen. In the strong Mott-insulating state, fermions on each site are nearly independent of each other, and thus the entropy per site is proportional to the logarithmic of the spin degeneracy. In the weak Mott-insulating state, we could think there is still a reminiscence of Fermi surface, which strongly suppresses the entropy contribution. Therefore, the liquid-like state is more ordered than the solid-like state in the intermediate temperature regime.

On the other hand, the Pomeranchuk effect does not occur in the low temperature regime ($T \ll \Delta_s$), where thermal fluctuations are not strong enough to suppress AF correlations. In this case, the AF correlations between adjacent sites lift spin degeneracy and lower the entropy in the strong Mott-insulating state. Consequently, the Pomeranchuk effect is prominent in the intermediate temperature regime.

High temperature regime $T > T_h$ In this case, not only spin fluctuations but also charge fluctuations are defrozen by thermal fluctuations $T > \Delta_c$. Charge fluctuations cannot be completely suppressed by U , and contribute most to the entropy. Therefore, increasing U lowers the entropy at a fixed T in the high temperature regime.

As for the SU(6) case, its behavior of entropy v.s. U and T is qualitatively identical to the SU(4) case. Nevertheless, the intermediate temperature regime of the for-

mer is broader than the latter, which means that the Pomeranchuk effect is more prominent.

B. The Pomeranchuk effect

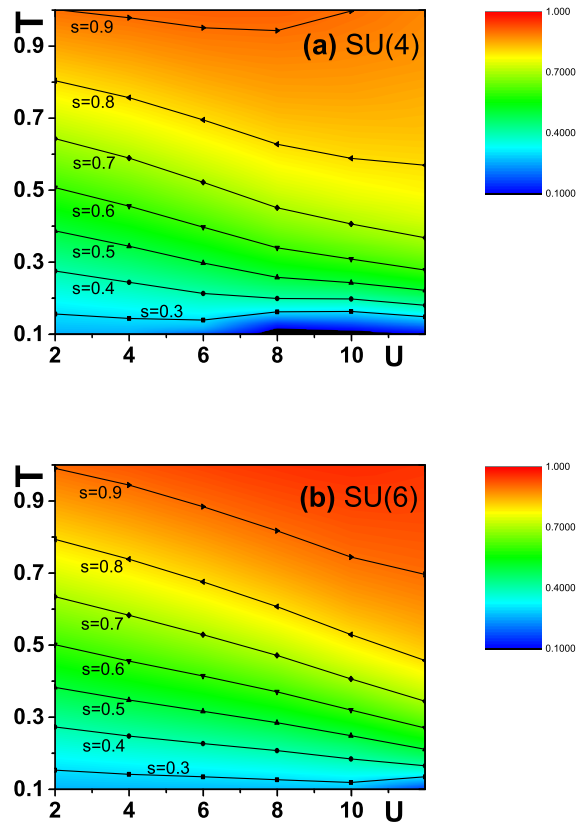


FIG. 3: The isoentropy curves for the half-filled (a) SU(4) and (b) SU(6) Hubbard models on a 10×10 square lattice. The entropy per particle $S_{SU(2N)}$ is indicated on each curve. (b) was published in Ref. [43], which is reproduced here with a new curve of $S_{SU(6)} = 0.3$ added.

As analyzed in section V A, in the strong Mott-insulating regime the lattice system has larger entropy capacity than in the weak Mott-insulating regime, which leads to the Pomeranchuk effect. This effect was first proposed in the ^3He system, where, in the low temperature region, increasing pressure adiabatically can further cool the system. In low temperature physics, this effect was employed as an effective cooling method named after Pomeranchuk. The similar situation occurs in the Hubbard model. Nevertheless, at low temperatures where the AF correlations are important, the spin degeneracy is lifted, which reduces the entropy in the Mott-insulating state. In this case, the Pomeranchuk effect does not occur. The DQMC simulations have been performed for the half-filled SU(2) Hubbard model in the

literature. Both in 2D and 3D cases, the Pomeranchuk effect is not obvious in the range of the entropy per particle $S_{SU(2)}$ between 0.1 to 0.9, even if the interaction achieves $U/t \sim 10^{40-42}$.

In the multi-component $SU(2N)$ Hubbard model, the situation is different. Due to the increase of the number of fermion components, the Pomeranchuk effect is greatly facilitated^{43,56}. The isoentropy curves v.s. U and T are plotted in Fig. 3 (a) and (b) for the $SU(4)$ and $SU(6)$ Hubbard models, respectively. In both cases, the Pomeranchuk effects are prominent in the intermediate temperature regime with intermediate interaction strengths, which emerge at $0.4 < S_{SU(4)} < 0.8$ for the $SU(4)$ case, and at $0.3 < S_{SU(6)} < 0.9$ for the $SU(6)$ case.

The enhancement of the Pomeranchuk effect can be illustrated by comparing the $SU(2)$ and $SU(4)$ cases. When deeply inside the Mott-insulating state, in the intermediate temperature regime, the AF correlations can be neglected, and the entropy per particle $S_{SU(2N)}$ is dominated by the contribution of spin degeneracy. Therefore, the entropy capacities can be estimated as $S_{SU(2)} = \ln 2 \approx 0.69$, which is smaller than $S_{SU(4)} = \ln(C_4^2)/2 \approx 0.89$. On the other hand, in the intermediate interaction regime, the charge gap in the $SU(4)$ case is significantly smaller than that in the $SU(2)$ case for the same interaction U . This means that fermions in the $SU(4)$ Hubbard model can be more easily excited to the upper Hubbard band than those in the $SU(2)$ case, which also enhances the entropy capacity of fermions in the $SU(4)$ case.

VI. THE PROBABILITY DISTRIBUTION OF THE ONSITE OCCUPATION NUMBER

To characterize charge fluctuations, we study the probability distribution of the onsite occupation number. In the $SU(2)$ case, at half filling the double-occupation number $n_d(i) = \langle n(i)_\uparrow n(i)_\downarrow \rangle$ is related to the local moment $\langle m_z^2 \rangle = 1 - 2n_d$, which exhibits a slightly non-monotonic behavior as a function of T for fixed U ⁵⁷. Also, in cold atom experiments, this quantity can be measured with *in situ* single-site resolution techniques^{58,59}. Let us consider the $SU(4)$ case. At half-filling the most probable configuration of onsite particle number is $n(i) = 2$. At finite U , particles are allowed to hop between different sites, leading to charge fluctuations. Due to particle-hole symmetry, the probabilities for the occupation numbers n and $2N - n$ are equal. Thus we only need to calculate $P(n)$ with $n = 0, 1$, and 2, respectively. They are defined

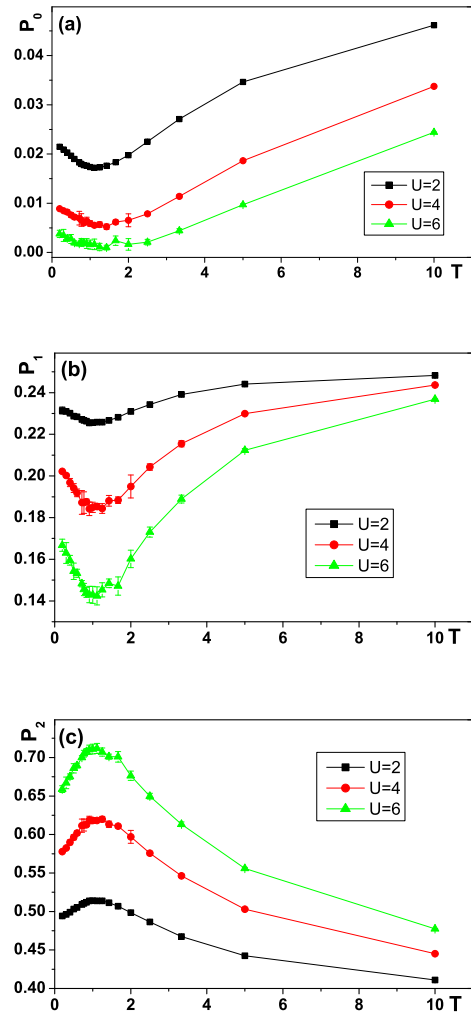


FIG. 4: The probabilities $P(n)$ for the onsite particle numbers (a) $P(0)$, (b) $P(1)$, and (c) $P(2)$ v.s. T and U in the half-filled $SU(4)$ Hubbard model. Due to the particle-hole symmetry, $P(0) = P(4)$, and $P(1) = P(3)$, and $2P(0) + 2P(1) + P(2) = 1$. The lattice size is $L \times L$ with $L = 10$.

as

$$\begin{aligned}
 P(0) &= \prod_{\alpha=1}^4 (1 - n_i^\alpha); \\
 P(1) &= \sum_{\alpha=1}^4 n_i^\alpha \prod_{\beta \neq \alpha} (1 - n_i^\beta); \\
 P(2) &= \sum_{\alpha \neq \beta} n_i^\alpha n_i^\beta \prod_{\gamma \neq \alpha \beta} (1 - n_i^\gamma). \quad (11)
 \end{aligned}$$

Obviously, they satisfy the relation $2P(0) + 2P(1) + P(2) = 1$.

The simulation results of $P(n)$ ($n = 0, 1$ and 2) as a function of T for various U are presented in Fig. 4. In the weak and intermediate interaction regimes, charge fluc-

tuations are significant. The maximal probability of the exact half-filling $P(2)$ only achieves around 70% when $U/t = 6$. In contrast, the probabilities of one-particle fluctuation defined by $2P(1)$ fall in the range between 30% and 40%. The probabilities of two-particle fluctuation, $2P(0)$, are typically as low as a few percent. Each $P(n)$ ($n = 0, 1$ and 2) exhibits non-monotonic behavior as T increases. For example, at low temperatures P_0 and P_1 fall with the increase of T ; then after reaching their minima at the temperature scale around t , they grow again. This indicates that in the temperature regime $T < t$, on-site charge fluctuations are suppressed with increasing T . This counterintuitive phenomenon reminds us of the Pomeranchuk effect, that the system tends to localize fermions in the intermediate temperature regime to maximize the entropy, which mainly comes from the spin degeneracy. When the temperature further increases, charge fluctuations are activated and grow with T .

VII. THE MAGNETIC PROPERTIES

In this section, we study the magnetic properties of the half-filled $SU(2N)$ ($2N=4$ and 6) Hubbard model on a square lattice at finite temperatures, including both the uniform spin susceptibilities and the AF structure factor.

A. The uniform spin susceptibilities

We now consider the uniform spin susceptibilities $\chi_{SU(2N)}$. Because the total spin is conserved, $\chi_{SU(2N)}$ can be expressed as the equal-time correlations through the structure factor at $\vec{q} = 0$:

$$\chi_{su(2N)}(T) = \frac{1}{k_B T} S_{SU(2N)}(\vec{q} = 0). \quad (12)$$

where the structure factor $S_{su(2N)}(\vec{q})$ is defined by Eq.(4).

In the 2D half-filled $SU(2)$ Hubbard model⁴², or, the Heisenberg model⁶⁰, it is known that at high temperatures, $\chi_{su(2)}$ behaves as the Curie-Weiss law which is proportional to $1/T$. At low temperatures, $\chi_{su(2)}(T)$ is suppressed due to the AF correlations, and therefore it exhibits a peak at a low temperature scale T_p . T_p can be used to roughly characterize the spin energy scale $T_p \simeq \Delta_s$ (in Heisenberg model $T_p \simeq J$).

The simulation results of the uniform spin susceptibilities for the $SU(4)$ and $SU(6)$ Hubbard models are presented in Figs. 5 (a) and (b), respectively. Only the weak and intermediate interaction regimes with $2 \leq U/t \leq 12$ are considered here. In the $SU(4)$ case, when $U/t < 6$, the energy scale of Δ_s is very small, and thus the peak location is beyond the temperature scope $T/t > 0.1$ in our simulations. Compared to the $SU(2)$ case, Δ_s in the $SU(4)$ case is significantly weakened. For example, the peak in the $SU(2)$ Hubbard model is located around

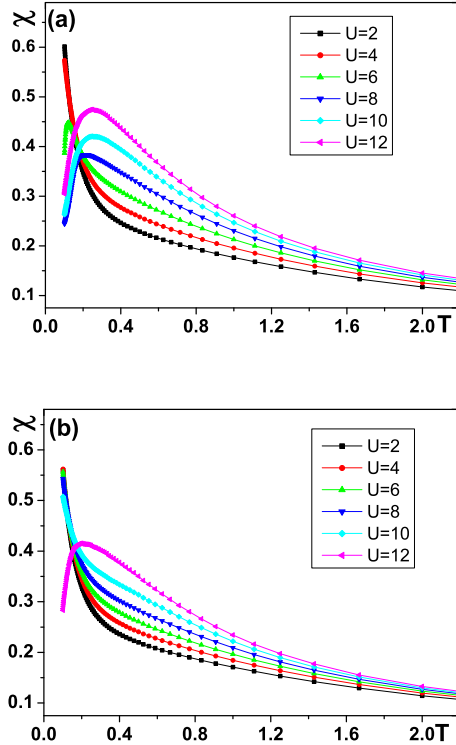


FIG. 5: The uniform spin susceptibilities v.s. T for various U in the half-filled (a) $SU(4)$ and (b) $SU(6)$ Hubbard models. The system size is $L \times L$ with $L = 10$. Error bars are smaller than the data points.

$T_p/t \approx 0.3$ when $U/t = 4$ as simulated in Ref. [43]. Nevertheless, the peak locations in the interaction regime $6 < U/t < 12$ have already become visible at temperatures $T_p/t > 0.1$. Furthermore, the magnitude of T_p and the peak of $\chi_{SU(4)}$ increases with U , which shows the enhancement of AF correlations. In the $SU(6)$ case, the AF correlations are further weakened compared to the $SU(4)$ case: among the curves in Fig. 5 (b), only the one with $U/t = 12$ exhibits a peak visible at temperatures $T_p/t > 0.1$. This indicates the weakening of the spin energy scale Δ_s in the intermediate interaction regime with increasing the number of fermion components.

B. AF structure factors

We use the AF structure factor $S_{SU(2N)}(\mathbf{Q})$ defined with staggered wave vector $\mathbf{Q} = (\pi, \pi)$ to describe the AF correlations. In Fig. 6 (a), the curves of the AF structure factor v.s. T are plotted at $U/t = 12$ in both the $SU(4)$ and $SU(6)$ cases. Both $S_{SU(4)}(\mathbf{Q})$ and $S_{SU(6)}(\mathbf{Q})$ increase monotonically with the decrease of T , which indicates the development of AF correlations. At a fixed T , $S_{SU(4)}(\mathbf{Q})$ is stronger than $S_{SU(6)}(\mathbf{Q})$, which becomes even more prominent at low temperatures. This is con-

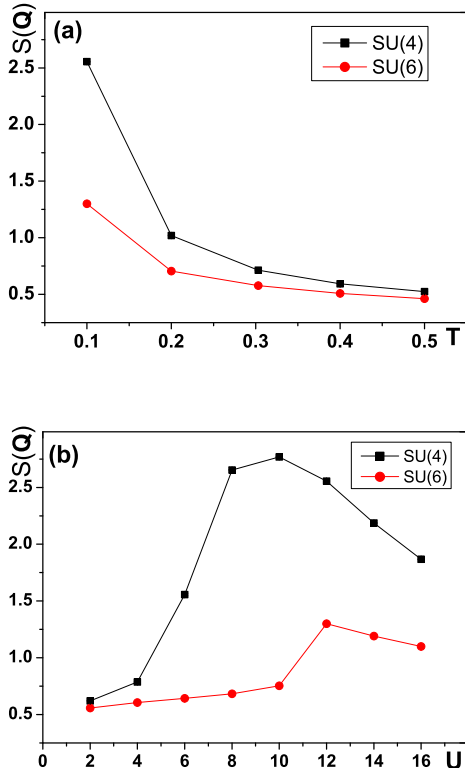


FIG. 6: The AF structure factors $S_{SU(2N)}(\mathbf{Q})$ with $\mathbf{Q} = (\pi, \pi)$: (a) as a function of T for fixed $U/t = 12$, and (b) as a function of U for fixed $T/t = 0.1$ for the half-filled SU(4) and SU(6) Hubbard models. The system size is $L \times L$ with $L = 10$. Error bars are smaller than the data points.

sistent with the picture that increasing the number of fermion components suppresses AF correlations.

In Fig. 6 (b), the dependence of $S_{SU(2N)}(\mathbf{Q})$ on U at a fixed temperature, $T/t = 0.1$, is plotted in both SU(4) and SU(6) cases, where the U -dependencies exhibit a non-monotonic behavior. At small U , $S_{SU(4)}(\mathbf{Q})$ and $S_{SU(6)}(\mathbf{Q})$ increase with U . In this weak interacting regime, $\Delta_c \simeq \Delta_s < T = 0.1t$, and thus increasing U enhances the spin energy scale but suppresses charge fluctuations, which facilitates to build up the AF correlation. Again, the enhancement of the AF correlation is more prominent in the SU(4) case than in the SU(6) case. An interesting feature is that the rates of increase jump at $U/t \approx 4$ in the SU(4) case, and at $U/t \approx 10$ in the SU(6) case. This may be due to a rapid increase of the charge energy scale Δ_c , which indicates the crossover from the weak interaction regime to the intermediate interaction regime. The AF in the weak interaction regime is due to Fermi surface nesting, and it evolves to the local moment physics as U enters the intermediate interaction regime. At large U , $\Delta_s \simeq J = 4t^2/U$ decreases with the increase of U . Thermal fluctuations are described by the parameter T/J , and thus increasing U effectively

enhances thermal fluctuations.

On the other hand, the zero temperature projector QMC results⁵⁵ show that the AF long-range orderings reach the maxima around $U/t \approx 8$ and 10 in the SU(4) and SU(6) cases, respectively. The AF ordering is then suppressed by further increasing U , which is an effect of quantum fluctuations. In the SU(6) case, the AF long-range order is even completely suppressed around $U/t \approx 15$ at zero temperature. This is because when deeply inside the Mott-insulating regime, the number of superexchange processes between two adjacent sites increases rapidly with the number of fermion components, which indicates the enhancement of quantum fluctuations. Combining both effects of quantum and thermal fluctuations, the AF correlations are weakened with increasing U in the strong interaction regime.

VIII. CONCLUSIONS

In summary, we have performed a systematic DQMC simulation study of thermodynamic properties of the half-filled SU($2N$) Hubbard model on a square lattice. Various thermodynamic behaviors including the entropy-temperature relation, the isoentropy curve and the probability distribution of the onsite occupation number have been simulated, which demonstrate the Pomeranchuk effect is facilitated with increasing fermion components. Based on the charge and spin energy scales, we have analyzed the thermodynamic properties in weak and strong interaction regimes. In the weak interaction regime, the physics is characterized by the Fermi surface nesting, while in the strong interaction regime the physics is mostly in the local moment picture. Additionally, in our simulations the uniform spin susceptibilities and the AF structure factors both exhibit qualitatively different behaviors in weak and strong interaction regimes. Theoretical analysis as well as DQMC simulations show that the interaction strength separating weak and strong interaction regimes increases with the number of fermion components.

Acknowledgments

Z.Z., C.W., and Y.W. acknowledges financial support from the National Natural Science Foundation of China under Grant No. 11328403, and the Fundamental Research Funds for the Central Universities. C.W. is supported by the NSF DMR-1410375 and AFOSR FA9550-14-1-0168. Z.C. acknowledges the support from SFB FoQuS (FWF Project No.F4006-N16) and the ERC Synergy Grant UQUAM.

Appendix: An exact Hubbard-Stratonovich decomposition for SU(4) and SU(6) Hubbard interactions

For the SU(2) case, the HS transformation is usually performed by using the discrete Ising fields^{47,48}. However, the decomposition in spin channel can not be easily generalized to the SU(2N) case due to the increase of spin components. Instead, we choose an discrete HS decomposition in the density channel at the price of involving complex numbers as used in Ref. [61]. The HS transformation for a half-filled SU(2N) Hubbard model reads:

$$e^{-\frac{\Delta\tau U}{2}(n_j - N)^2} = \frac{1}{4} \sum_{l=\pm 1, \pm 2} \gamma_j(l) e^{in_j(l)(n_j - N)}, \quad (13)$$

where two sets of discrete HS fields γ and η are employed.

However, the HS decomposition with an error of order $(\Delta\tau)^4$ in Ref.[61] is not exact. In Ref.[55], a new HS decomposition was proposed with a new set of parameters, which is exact for the SU(4) and SU(6) Hubbard interactions. The Ising fields are defined as follows

$$\begin{aligned} \gamma(\pm 1) &= \frac{-a(3 + a^2) + d}{d}; \\ \gamma(\pm 2) &= \frac{a(3 + a^2) + d}{d}; \\ \eta(\pm 1) &= \pm \cos^{-1} \left\{ \frac{a + 2a^3 + a^5 + (a^2 - 1)d}{4} \right\}; \\ \eta(\pm 2) &= \pm \cos^{-1} \left\{ \frac{a + 2a^3 + a^5 - (a^2 - 1)d}{4} \right\} \end{aligned}$$

where $a = e^{-\Delta\tau U/2}$, and $d = \sqrt{8 + a^2(3 + a^2)^2}$.

-
- * Electronic address: yu.wang@whu.edu.cn
- ¹ I. Affleck and J. B. Marston, Phys. Rev. B **37**, 3774 (1988).
 - ² D. P. Arovas and A. Auerbach, Phys. Rev. B **38**, 316 (1988).
 - ³ N. Read and S. Sachdev, Phys. Rev. B **42**, 4568 (1990).
 - ⁴ N. Read and S. Sachdev, Phys. Rev. Lett. **66**, 1773 (1991).
 - ⁵ S. Sachdev and N. Read, Int. J. Mod. Phys. B **5**, 219 (1991).
 - ⁶ K. Harada, N. Kawashima, and M. Troyer, Phys. Rev. Lett. **90**, 117203 (2003).
 - ⁷ F. F. Assaad, Phys. Rev. B **71**, 75103 (2005).
 - ⁸ P. Corboz, A. M. Läuchli, K. Penc, M. Troyer, and F. Mila, Phys. Rev. Lett. **107**, 215301 (2011).
 - ⁹ P. Corboz, M. Lajkó, A. M. Läuchli, K. Penc, and F. Mila, Phys. Rev. X **2**, 041013 (2012).
 - ¹⁰ A. Paramekanti and J. B. Marston, J. Phys. Cond. Matt. **19**, 125215 (2007).
 - ¹¹ C. Wu, J. P. Hu, and S. C. Zhang, Phys. Rev. Lett. **91**, 186402 (2003).
 - ¹² C. Wu, Mod. Phys. Lett. B **20**, 1707 (2006).
 - ¹³ A. V. Gorshkov, M. Hermele, V. Gurarie, C. Xu, P. S. Julienne, J. Ye, P. Zoller, E. Demler, M. D. Lukin, and A. M. Rey, Nature Phys. **6**, 289 (2010).
 - ¹⁴ C. Wu, Nature Physics **8**, 784785 (2012).
 - ¹⁵ S. Taie, Y. Takasu, S. Sugawa, R. Yamazaki, T. Tsujimoto, R. Murakami, and Y. Takahashi, Phys. Rev. Lett. **105**, 190401 (2010).
 - ¹⁶ B. J. DeSalvo, M. Yan, P. G. Mickelson, Y. N. Martinez de Escobar, and T. C. Killian, Phys. Rev. Lett. **105**, 030402 (2010).
 - ¹⁷ H. Hara, Y. Takasu, Y. Yamaoka, J. M. Doyle, and Y. Takahashi, Phys. Rev. Lett. **106**, 205304 (2011).
 - ¹⁸ S. Taie, R. Yamazaki, S. Sugawa, and Y. Takahashi, Nature Physics **8**, 825 (2012).
 - ¹⁹ F. Scazza, C. Hofrichter, M. Hofer, P. C. D. Groot, I. Bloch, and S. Fölling, Nature Physics **8**, 825 (2014).
 - ²⁰ X. Zhang, M. Bishof, S. L. Bromley, C. V. Kraus, M. S. Safronova, P. Zoller, A. M. Rey, and J. Ye, ArXiv e-prints (2014), 1403.2964.
 - ²¹ G. Pagano, M. Mancini, G. Cappellini, P. Lombardi, F. Schafer, H. Hu, X.-J. Liu, J. Catani, C. Sias, M. Inguscio, et al., Nature Physics **10**, 198 (2014).
 - ²² P. Lecheminant, E. Boulat, and P. Azaria, Phys. Rev. Lett. **95**, 240402 (2005).
 - ²³ C. Honerkamp and W. Hofstetter, Phys. Rev. Lett. **92**, 170403 (2004).
 - ²⁴ C. Honerkamp and W. Hofstetter, Phys. Rev. B **70**, 094521 (2004).
 - ²⁵ L. He, M. Jin, and P. Zhuang, Phys. Rev. A **74**, 033604 (2006).
 - ²⁶ R. W. Cherg, G. Refael, and E. Demler, Phys. Rev. Lett. **99**, 130406 (2007).
 - ²⁷ A. Rapp, G. Zarand, C. Honerkamp, and W. Hofstetter, Phys. Rev. Lett. **98**, 160405 (2007).
 - ²⁸ A. Rapp, W. Hofstetter, and G. Zarand, Phys. Rev. Lett. **77**, 144520 (2008).
 - ²⁹ C. Wu, Phys. Rev. Lett. **95**, 266404 (2005).
 - ³⁰ M. A. Cazalilla, A. F. Ho, and M. Ueda, New J. Phys. **11**, 103033 (2009).
 - ³¹ S. R. Manmana, K. R. A. Hazzard, G. Chen, A. E. Feiguin, and A. M. Rey, Phys. Rev. A **84**, 043601 (2011).
 - ³² H.-H. Hung, Y. Wang, and C. Wu, Phys. Rev. B **84**, 054406 (2011).
 - ³³ E. Szirmai and M. Lewenstein, Europhys. Lett. **93**, 66005 (2011).
 - ³⁴ G. Szirmai, E. Szirmai, A. Zamora, and M. Lewenstein, Phys. Rev. A **84**, 011611 (2011).
 - ³⁵ M. Hermele, V. Gurarie, and A. M. Rey, Phys. Rev. Lett. **103**, 135301 (2009).
 - ³⁶ M. Hermele and V. Gurarie, Phys. Rev. B **84**, 174441 (2011).
 - ³⁷ C. Xu, Phys. Rev. B **81**, 144431 (2010).
 - ³⁸ J. Heinze, J. S. Krauser, N. Fläschner, K. Sengstock, C. Becker, U. Ebling, A. Eckardt, and M. Lewenstein, Phys. Rev. Lett. **110**, 250402 (2013).
 - ³⁹ F. Werner, O. Parcollet, A. Georges, and S. R. Hassan, Phys. Rev. Lett. **95**, 056401 (2005).
 - ⁴⁰ A.-M. Daré, L. Raymond, G. Albinet, and A.-M. S. Tremblay, Phys. Rev. B **76**, 064402 (2007).
 - ⁴¹ T. Paiva, R. Scalettar, M. Randeria, and N. Trivedi, Phys.

- Rev. Lett. **104**, 066406 (2010).
- ⁴² T. Paiva, Y. L. Loh, M. Randeria, R. T. Scalettar, and N. Trivedi, Phys. Rev. Lett. **107**, 086401 (2011).
- ⁴³ Z. Cai, H.-h. Hung, L. Wang, D. Zheng, and C. Wu, Phys. Rev. Lett. **110**, 220401 (2013).
- ⁴⁴ E. Fradkin, *Field theories of condensed matter systems* (Cambridge University Press, Cambridge, 2013).
- ⁴⁵ K. R. A. Hazzard, A. M. Rey, and R. T. Scalettar, Phys. Rev. B **87**, 035110 (2013).
- ⁴⁶ R. Blankenbecler, D. J. Scalapino, and R. L. Sugar, Phys. Rev. D **24**, 2278 (1981).
- ⁴⁷ J. E. Hirsch, Phys. Rev. B **28**, 4059 (1983).
- ⁴⁸ J. E. Hirsch, Phys. Rev. B **31**, 4403 (1985).
- ⁴⁹ S. R. White, D. J. Scalapino, R. L. Sugar, E. Y. Loh, J. E. Gubernatis, and R. T. Scalettar, Phys. Rev. B **40**, 506 (1989).
- ⁵⁰ R. R. D. Santos, Braz. J. Phys. **33**, 36 (2003).
- ⁵¹ D. J. Scalapino, ArXiv Condensed Matter e-prints (2006), arXiv:cond-mat/0610710.
- ⁵² K. Binder and D. Heermann, *Monte Carlo Simulation in Statistical Physics* (Springer, Berlin, 1997).
- ⁵³ M. Suzuki, *Quantum Monte Carlo Methods* (Springer, Berlin, 1986).
- ⁵⁴ J. E. Hirsch and S. Tang, Phys. Rev. Lett. **62**, 591 (1989).
- ⁵⁵ D. Wang, Y. Li, Z. Cai, Z. Zhou, Y. Wang, and C. Wu, Phys. Rev. Lett. **112**, 156403 (2014).
- ⁵⁶ K. R. A. Hazzard, V. Gurarie, M. Hermele, and A. M. Rey, Phys. Rev. A **85**, 041604 (2012).
- ⁵⁷ T. Paiva, R. T. Scalettar, C. Huscroft, and A. K. McMahhan, Phys. Rev. B **63**, 125116 (2001).
- ⁵⁸ W. S. Bakr, A. Peng, M. E. Tai, R. Ma, J. Simon, J. I. Gillen, S. Fölling, L. Pollet, and M. Greiner, Science **329**, 547 (2010).
- ⁵⁹ J. F. Sherson, C. Weitenberg, M. Endres, M. Cheneau, I. Bloch, and S. Kuhr, Nature **467**, 68 (2010).
- ⁶⁰ M. S. Makivić and H.-Q. Ding, Phys. Rev. B **43**, 3562 (1991).
- ⁶¹ F. F. Assaad, ArXiv Condensed Matter e-prints (1998), arXiv:cond-mat/9806307.